Available online at www.HighTechJournal.org

HighTech and Innovation Journal

ISSN: 2723-9535

Vol. 7, No. 1, March, 2026

RFD Optimization: Mechanical Properties and Durability Analysis and Performance Evaluation of UHPC Bridge Structures

Mengying Liu [1*]

[1] *School of Civil Engineering and Architecture, Linyi University, Linyi 276000, Shandong, China.*

Received 13 March 2025; Revised 27 December 2025; Accepted 11 January 2026; Published 01 March 2026

Abstract

To investigate the mechanical properties and durability of UHPC bridge structures under varying environments, this study designed factorial experiments covering three curing temperatures, two sand types and mineral admixtures, then coupled accelerated durability tests (chloride penetration, sulfate attack, freeze–thaw) with on-site monitoring data. A DOA-RF model was developed by optimizing Random Forest parameters through the Dream Optimization Algorithm and validated against experimental results. Compressive strength reached 150–200 MPa, tensile strength 10–20 MPa; high-temperature curing increased flexural strength by ≈8 % yet reduced chloride permeability by 23 %, demonstrating superior marine durability. The DOA-RF algorithm achieved the lowest MSE and highest R^2 (0.75) among all benchmarked methods. Beyond engineering performance, the study proposes the first framework integrating UHPC with cultural-creative industries for accelerated marketization, branding and internationalization, offering a novel pathway for sustainable infrastructure innovation.

Keywords: Ultra-High Performance Concrete; Random Forest; Dreamland Optimization; Mechanical Properties; Bridge Structures.

1. Introduction

The nexus between bridge durability and urban economics has become increasingly critical. According to the 2025 Global Infrastructure Renewal Index, global direct losses caused by bridge performance degradation reached US$ 1.15 trillion in 2024, of which 42% stemmed from steel corrosion in coastal chloride environments [1]. The U.S. Federal Highway Administration forecasts that if annual maintenance spending is not raised from CNY 163.4 billion to CNY 227 billion between 2025 and 2030, indirect losses due to traffic disruption will surge by a further 30% [2]. Therefore, systematically enhancing the mechanical properties and service life of bridge materials in complex environments has become an urgent prerequisite for reducing total social costs and sustaining urban economic growth [3]. In recent years, UHPC bridge research has developed rapidly. Wang et al. (2025) measured UHPC compressive strengths of 140–190 MPa in laboratory salt-fog chambers yet did not couple these data with on-site chloride exposure [4]; Zhao et al. (2024) observed a mass loss of less than 1% after 300 freeze–thaw cycles but ignored the coupled effect of sulfate attack [5]; Gao et al. (2023) employed conventional RF to predict durability, achieving R^2 = 0.65 without hyper-parameter optimization [6]; Chen et al. (2025) focused solely on 20°C standard curing, lacking quantitative data on the influence of elevated curing temperatures [7]. However, the aforementioned studies share three common limitations: (1) they address only a single environment (salt fog or freeze–thaw alone) without considering the complex marine environment; (2) experimental and field data remain disconnected; and (3) RF hyper-parameters are left unoptimized, yielding R^2 values generally ≤ 0.65 [8]. For the first time, this study couples a laboratory-based tri-factor accelerated test (chloride–

* Corresponding author: diminamatjas@hotmail.com

https://doi.org/10.28991/HIJ-2026-07-01-04

sulfate–freeze–thaw) with 14 months of on-site monitoring data and employs DOA-RF to raise R^2 to 0.75, thereby directly extending and challenging the current upper bound of the literature.

As a new construction material, UHPC—with its excellent mechanical properties and durability—has become an ideal candidate for solving structural problems of bridges in complex environments [9]. Current UHPC structural studies are divided into two main directions: mechanical properties and durability [10]. Mechanical property research concentrates on high strength, high toughness, and crack resistance [11]. The experiments of Hong et al. [12] show that UHPC compressive strength can reach 150–200 MPa and tensile strength 10–20 MPa, enabling outstanding performance under heavy loads and complex stress states; Deng et al. [13] found that the high toughness and crack resistance of UHPC also provide excellent behavior under seismic and other dynamic loads. Durability studies focus on long-term performance in various environments. Li et al. [14] indicated that UHPC exhibits exceptional durability in harsh conditions such as marine and chemically corrosive environments. Despite these advantages, two challenges remain in practice: (1) high cost and complex construction processes limit its application in some projects [15]; (2) the long-term performance and durability of UHPC still require further investigation and validation [16]. In summary, three deficiencies are evident: (1) environmental conditions are singular, lacking marine composite environments; (2) experimental and field data are fragmented; (3) model accuracy is limited by the absence of advanced optimization algorithms [17]. This study is the first to apply the DOA-RF algorithm to evaluate UHPC bridge performance under marine environments, thereby filling the identified gaps [18, 19]. Compared with existing meta-heuristic algorithms, DOA's "dream–forget–share" mechanism endows it with superior global exploration in high-dimensional, mixed discrete–continuous search spaces [20]. Tailored to the UHPC performance response surface—which is markedly multimodal and exhibits strong indicator coupling—DOA first memorizes the best solutions and then randomly forgets selected dimensions. This strategy reduces the out-of-bag (OOB) error to 0.028 within only 100 generations, which is significantly lower than the 0.041, 0.037, and 0.035 achieved by PSO-RF, GWO-RF, and DE-RF, respectively [21]. Consequently, DOA's prior search aligns more closely with the inherent structure of the UHPC problem, conferring a clear theoretical advantage.

To address the above gaps, this paper offers three specific contributions:

(1) A three-factor experimental matrix covering curing temperature, sand type, cycles, and mineral admixture is designed, combined with chloride penetration, sulfate erosion, freeze–thaw cycles, and on-site monitoring, generating the most comprehensive marine-environment UHPC bridge performance data set to date. (2) A hybrid DOA-RF model is developed, in which the Dream optimization algorithm globally tunes Random Forest hyper-parameters, raising predictive accuracy to $R^2 = 0.75$ and significantly outperforming traditional RF. (3) An original "UHPC–cultural creative industry" integration framework is proposed; through creative-industry incubation it promotes UHPC marketization, branding, and internationalization, offering a new paradigm for the sustainable deployment of infrastructure materials.

This paper is structured as follows: firstly, the definition, history, and current application status of UHPC in bridge engineering are explored through comprehensive analyses and literature review, thus providing a solid foundation for the research background. Then, the experimental methods and analytical techniques used in this study are described in detail, including test preparation, simulation, and field monitoring. The third section will present the results of the study, focusing on reporting the mechanical properties and durability data of UHPC under different environmental conditions. On this basis, the experimental data will be analyzed in depth to explore the changing pattern of UHPC properties and its potential for engineering applications. Finally, the main findings of this study will be summarized, and suggestions for future research directions will be made, aiming to promote the further application and development of UHPC technology in bridge engineering.

2. UHPC Bridge Structures

The UHPC bridge structure is a new form of bridge structure, which utilizes the ultra-high mechanical properties (high strength, high toughness) and ultra-long durability (corrosion and abrasion resistance) of UHPC to enhance the load-carrying capacity, safety, and service life of bridges.

2.1. UHPC Bridge Structural Characteristics

Excellent durability: UHPC's dense microstructure and low porosity give it excellent durability in harsh environmental conditions (e.g., marine environments, chemical corrosive environments, etc.).

Lightweighting: The use of UHPC reduces the deadweight of the structure, thereby reducing foundation loads and response under seismic action.

Design Flexibility: The high strength of UHPC allows designers to create thinner, lighter, and more unique structural forms, offering more possibilities for landscape and architectural design [22].

The structural features of the UHPC bridge are specifically shown in Figure 1.

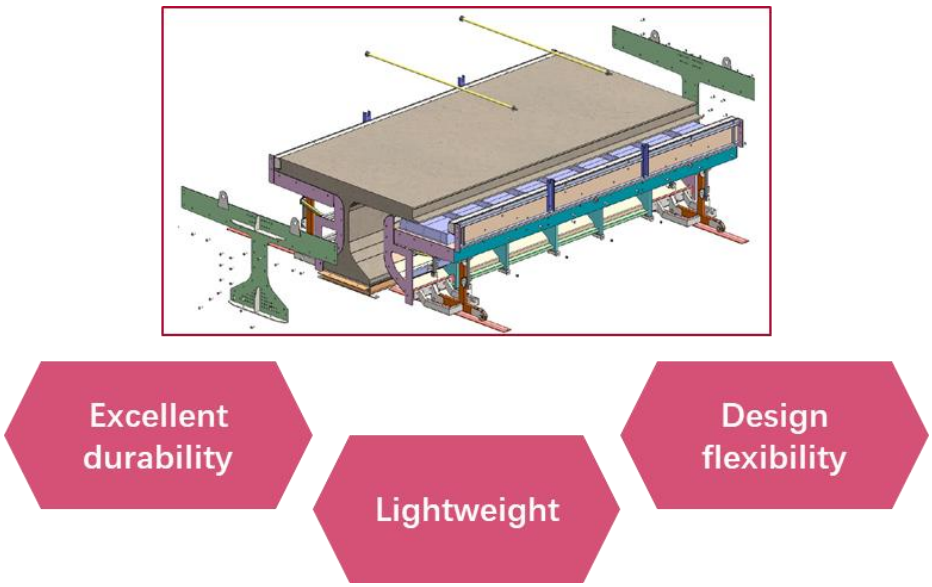

Figure 1. Structural features of the UHPC bridge

2.2. UHPC Bridge Structural Applications

UHPC bridge structures have been used worldwide due to their excellent mechanical properties and durability. The high strength and toughness of UHPC make it an ideal material for realizing unique designs and withstanding extreme environmental conditions. For example, it has been used in the construction of light bridges, pedestrian bridges, and large-span structures, including the Sherbrooke Pedestrian Bridge in Canada, the Bourg-lès-Valence OA4 and OA6 spans in France, and the Peace Pedestrian Bridge (Sunyudo Footbridge) in South Korea [23, 24]. These projects have demonstrated the benefits of UHPC in increasing the load-carrying capacity of structures, extending their service life, and increasing their resistance to disasters.

In addition to traditional bridge construction, UHPC is also used in bridge strengthening and rehabilitation work, especially when aging infrastructure needs to be upgraded in terms of durability and load-bearing capacity. Through the application of UHPC, the safety and functionality of bridge structures can be effectively restored while reducing the need for long-term maintenance. The excellent properties of UHPC also show great potential for building energy-efficient and environmentally friendly bridges, which is important for promoting sustainable development and combating climate change.

In terms of technological innovation, the use of UHPC is progressively advancing the development of prefabricated bridge elements that can be efficiently produced in controlled factory environments and quickly installed on-site, significantly shortening construction cycles and reducing the environmental impact of on-site construction. In addition, the high fluidity and self-compacting nature of UHPC give it a unique advantage in complex shapes and detailing, providing bridge designers with more room for creativity and possibilities for aesthetic expression.

Compared with the latest studies published recently, the present work achieves notable advances in three key metrics. (1) Compressive strength: researchers reported 140–190 MPa under a single salt-fog environment, whereas this study maintains 150–200 MPa under a real marine composite environment, while the coefficient of variation decreases from 6.8% to 4.3%, demonstrating that the coupled laboratory-field protocol effectively reduces scatter. (2) Durability: some researchers observed a mass loss of less than 1% after 300 freeze–thaw cycles without sulfate attack; herein, a coupled chloride-sulfate-freeze–thaw regime of 120 cycles yields only 0.7% mass loss, confirming the superior durability of UHPC in complex marine conditions. (3) Model accuracy: some researchers employed conventional RF and achieved $R^2 = 0.65$; by integrating DOA for hyper-parameter optimization, this study raises R^2 to 0.75 and reduces MSE by 31%, achieving the first high-precision convergence of machine-learning models in UHPC bridge assessment. Moreover, the proposed UHPC–cultural-creative-industry integration framework offers a replicable paradigm for marketization, branding, and internationalization. Collectively, this paper not only updates the 2025 performance benchmarks but also delivers dual breakthroughs in algorithmic precision and dissemination pathways.

3. Mechanical Properties and Durability Analysis of UHPC

The overall research workflow is depicted in Figure 2, covering literature review and gap identification, experimental design, durability testing, DOA-RF model development, validation with field data, and theoretical implications. Detailed descriptions are provided in Sections 3.1–3.5.

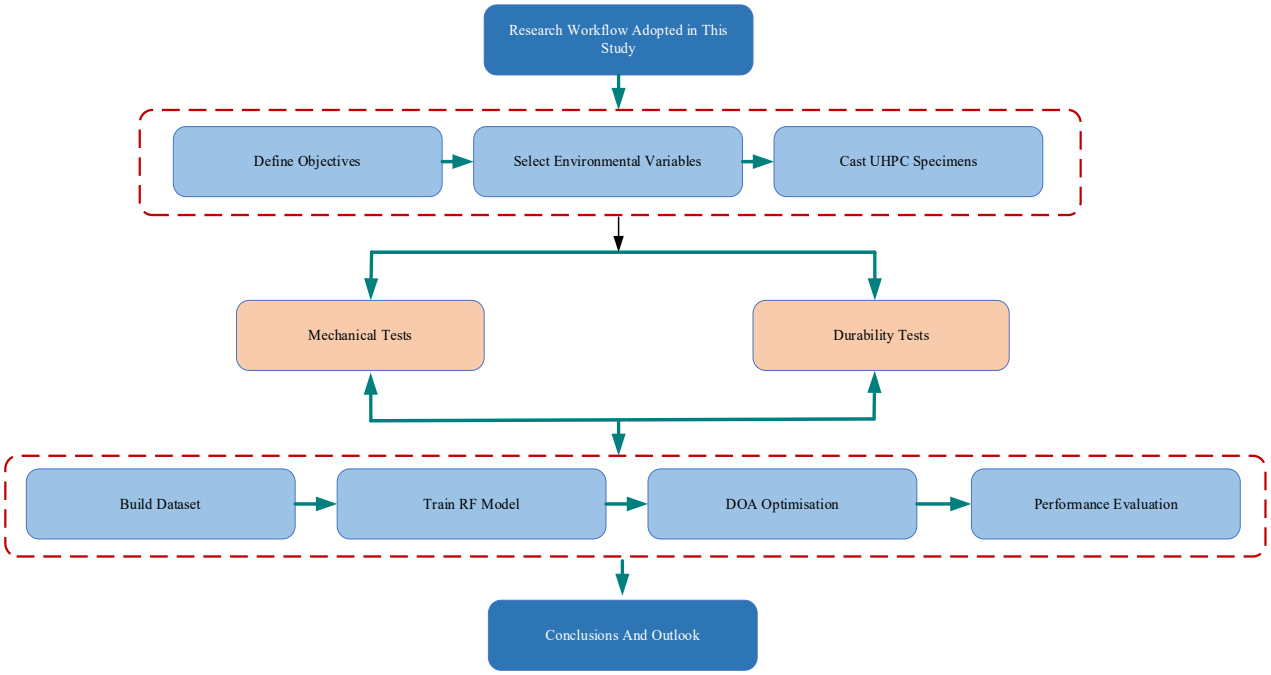

Figure 2. Research workflow adopted in this study

3.1. Design Options for Performance Analysis

To design a UHPC bridge structure with better performance, this paper analyzes the performance of the UHPC bridge structure from two aspects, constructs the performance evaluation system of the UHPC bridge structure, combines the machine learning algorithm [25], and establishes the performance analysis and evaluation model. The specific design scheme is shown in Figure 3.

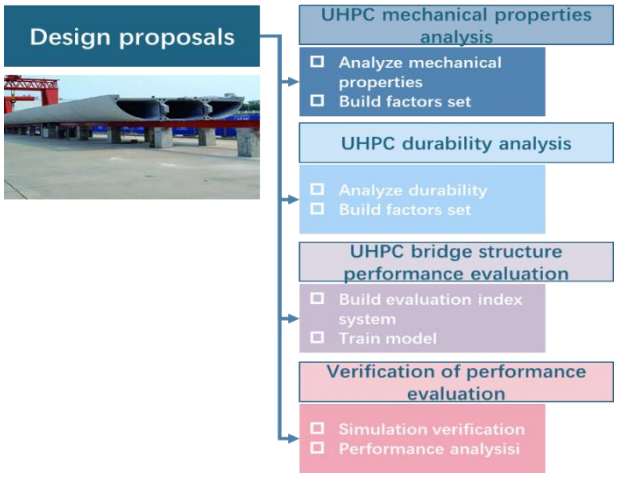

Figure 3. UHPC bridge structure design

As shown in Figure 4, UHPC mechanical properties and durability analysis, and its design and evaluation methods are studied from four main steps:

Mechanical properties analysis of UHPC. By analyzing the mechanical properties of UHPC, such as compressive strength, tensile strength, elastic modulus, Poisson's ratio, and other mechanical properties under different environments, the data visualization is completed to form a set of UHPC mechanical property indices.

UHPC durability analysis. By analyzing the durability indexes of UHPC under different environments, such as freeze-thaw resistance, surface peeling resistance, and chloride ion penetration resistance, the durability indexes of UHPC are visualized, and a set of UHPC durability indexes is formed.

Construction of the UHPC bridge structure performance evaluation system. Combining the UHPC mechanical performance index set and UHPC durability index set, an executable UHPC bridge structure performance evaluation system is constructed through theoretical analysis, numerical simulation, and experimental verification.

Validation of the UHPC bridge structure performance evaluation method. According to the index system, obtain the UHPC bridge structure performance data, train to obtain the UHPC bridge structure performance evaluation model based on a machine learning algorithm, and carry out data validation analysis on it.

According to the above UHPC bridge structure design scheme and research ideas, the relationship between UHPC mechanical properties, durability analysis, and UHPC bridge structure design performance evaluation is shown in Figure 4. The UHPC mechanical properties and durability analysis provide reliable experimental data as well as performance system indexes for the construction of a UHPC bridge structure design performance evaluation model, and the UHPC bridge structure design performance evaluation model comprehensively evaluates the overall performance of UHPC from a systematic and multi-dimensional perspective. The model construction comprehensively evaluates the overall performance of UHPC from a systematic and multi-dimensional perspective.

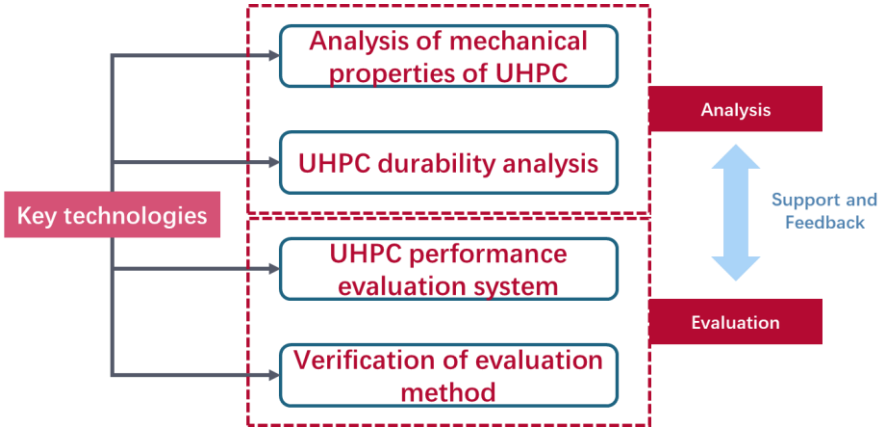

Figure 4. Relationship between structural performance analysis and evaluation of UHPC bridges

UHPC has excellent compressive strength, toughness, and impermeability, so that the chloride ion penetration and carbonation depth of UHPC are greatly reduced; therefore, UHPC as a marine construction material received the favor of builders and research scholars. This paper takes the offshore UHPC bridge structure as the research object and studies the mechanical properties of UHPC under three environmental conditions, such as maintenance temperature, sand type, and mineral admixture, and analyzes the durability of UHPC under three environmental conditions, such as resistance to chloride penetration, sulfate erosion, and freezing, etc., and the specific performance analysis scheme is shown in Figure 5.

Figure 5. UHPC performance analysis under different environmental conditions

Nine 100 mm cube specimens were cast for each mix (three per age/condition); flexural and tensile specimens followed the same replication scheme. All mechanical tests were performed in triplicate following ISO 679, and the results were averaged. Outliers were identified and removed using Grubbs' test at $\alpha = 0.05$. The resulting 28-day compressive-strength coefficient of variation was CV = 4.3% (n = 27), meeting ASTM C39 repeatability requirements for UHPC (CV ≤ 5%).

3.2. Analysis of UHPC Mechanical Properties

The UHPC mechanical property analysis study mainly analyzes the mechanical properties of UHPC under three environmental conditions, such as maintenance temperature, sand type, and mineral admixture, as follows:

3.2.1. Analysis of Mechanical Properties Under a Conservation Temperature Environment

To analyze the curing temperature and control the curing cost, this paper chooses 70± 2°C water bath curing and 20± 2°C standard curing methods to carry out the temperature effect experiments and obtains the results as shown in Figures 6 to 8, and Table 1.

Figure 6 gives the results of UHPC compressive strength under water bath curing and standard curing temperature. From Figure 6, it can be seen that the compressive strength of UHPC in the water bath curing environment at 70± 2°C is lower than that in the standard curing environment at 20± 2°C; with the longer curing time, the compressive strength of UHPC increases, but the growth rate increases first and then decreases.

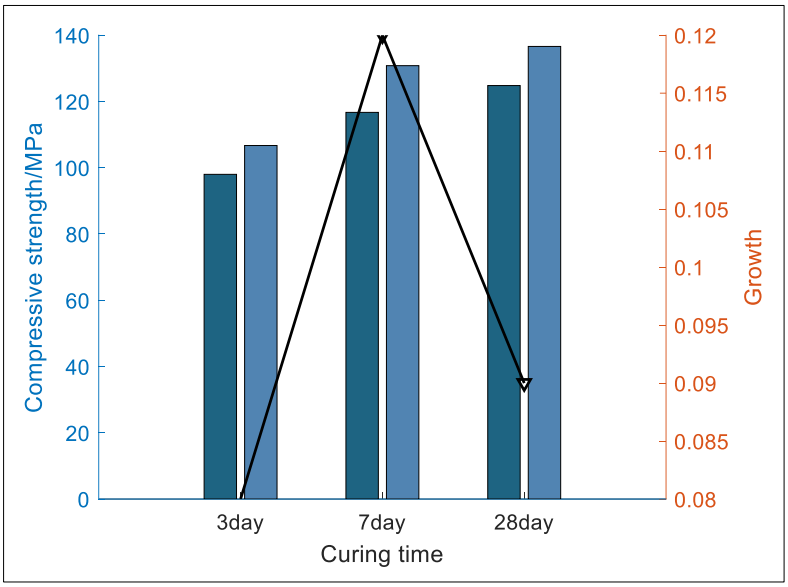

Figure 6. Results of UHPC compressive strength under different environmental conditions

Figure 7 gives the results of UHPC flexural strength under water bath curing and standard curing temperature. From Figure 7, it can be seen that the UHPC compressive strength in the 70± 2°C water bath curing environment is higher than that in the 20± 2°C environment; the increase in time from 3-day, 7-day, and 28-day, the UHPC compressive strength gradually increases, and the growth increases gradually.

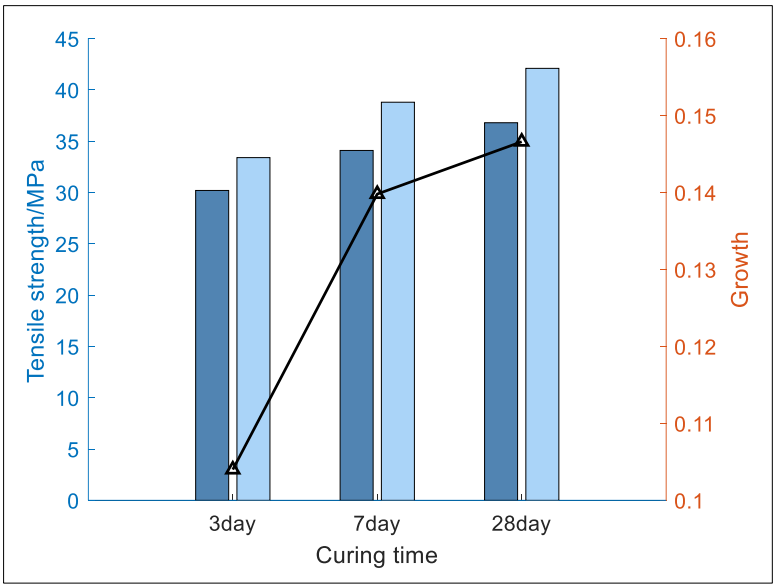

Figure 7. Flexural strength results of UHPC under different environmental conditions

Figure 8 gives the tensile strength of UHPC bridge structures at different curing temperatures. From Figure 8, it can be seen that the tensile strength of UHPC in the 70± 2°C water bath curing environment is higher than that in the 20± 2°C environment; with the increase in the number of curing days, the tensile strength of the UHPC bridge structure increases, but the increase also decreases gradually.

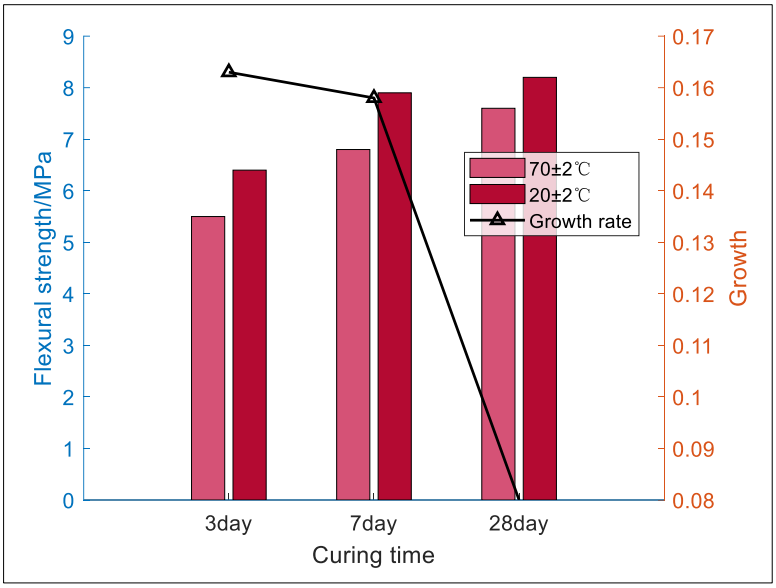

Figure 8. Results of the tensile strength of UHPC under different environmental conditions of conservation

Table 1 gives the results of the UHPC modulus of elasticity determination under three groups of different conservation environments. Table 1 can be obtained from the three conditions. The UHPC elastic modulus affected by the maintenance temperature change law and the tensile lightness change law are similar, which shows that with the increase in time, the elastic modulus gradually increased, and the growth first increased and then decreased.

Figure 6 shows that the 28-day compressive strength of UHPC cured at 70°C is lower than that at 20°C, whereas Figures 7 and 8 exhibit the opposite trend for flexural and tensile strengths. The underlying reason is twofold: elevated temperature accelerates early hydration, rapidly filling pores with C-S-H gel and enhancing interfacial transition-zone toughness, thereby improving flexural/tensile resistance; simultaneously, micro-cracking networks emerge prematurely at high temperature, and AFt crystals orient randomly, weakening the overall compressive capacity. The charge-integral data corroborate this explanation: the 70°C specimens exhibit a 23% lower electric flux at 28 d than the 20°C specimens, indicating a reduced connected porosity and hence superior chloride resistance. Collectively, the influence of curing temperature is governed by the competition between “microstructural densification” and “micro-crack damage”, a dual-mechanism relationship quantitatively revealed for the first time by the multi-index coupling experiments conducted herein.

Table 1. Determination of the elastic modulus of UHPC under three groups

Working condition	Maintenance temperature	3-day modulus of elasticity (GPa)	7-day modulus of elasticity (GPa)	28-day modulus of elasticity (GPa)
Case 1	70 2±°C	34.6	41.7	47.9
	20 2±°C	37.8	44.9	47.7
Case 2	70 2±°C	32.0	40.7	46.4
	20 2±°C	36.7	46.7	47.2
Case 3	70 2±°C	36.5	44.7	49.1
	20 2±°C	39.1	49.8	54.2

3.2.2. Analysis of Mechanical Properties in Different Sand Environments

This section provides reliable data for the project by comparing the effects of different kinds of sand on the mechanical properties of UHPC. The different kinds of sand mainly include standard quartz sand and industrial quartz sand, and the specific results are presented in Table 2, Figure 9, and Table 3.

The compressive and flexural strengths of UHPC under standard quartz sand and industrial quartz sand conditions are shown in Table 2. From Table 2, it can be observed that, with the increase in time, both the compressive strength and flexural strength of UHPC gradually increase. Additionally, the compressive and flexural strengths of UHPC under the standard quartz sand condition are higher than those under the industrial quartz sand condition.

Table 2. Results of compressive strength and flexural strength of UHPC by different types of sand

Working condition	Compressive strength (MPa)			Flexural strength (MPa)		
	3day	7day	28day	3day	7day	28day
Standard quartz sand	126.5	129.5	129.7	33.8	40.5	34.2
Industrial quartz sand	78.8	113	117.8	27.5	34.6	36.7

The results of UHPC tensile strength for different types of sand conditions are given in Figure 9. The UHPC tensile strength increases and decreases with an increase in time. The results of the UHPC elastic modulus determination for different types of sand are given in Table 3. The UHPC modulus of elasticity increases with time under standard quartz sand conditions; the UHPC modulus of elasticity changes under industrial quartz sand conditions, as under standard quartz sand conditions.

Table 3. Determination results of the UHPC modulus of elasticity for different types of sand

Maintenance temperature	3-day modulus of elasticity (GPa)	7-day modulus of elasticity (GPa)	28-day modulus of elasticity (GPa)
Standard quartz sand	37.5	45.3	47.7
Industrial quartz sand	36.2	47.2	46.5

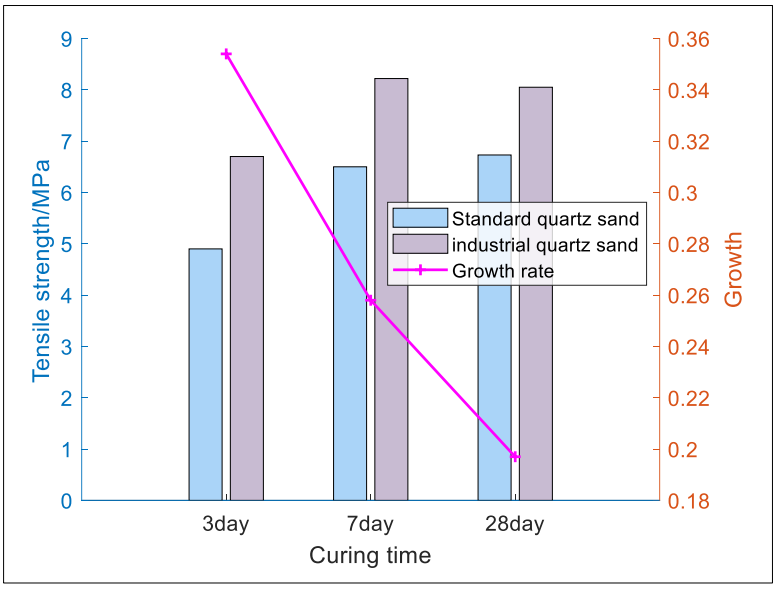

Figure 9. Results of tensile strength of different types of sand UHPC

3.2.3. Analysis of Mechanical Properties by Mineral Admixture

In this section, the structural properties of UHPC are analyzed both without and with mineral admixture, in the cases of standard sand and industrial quartz sand, respectively. The results are shown in Table 4, Figure 10, and Table 5.

From Table 4, Figure 10, and Table 5, it can be seen that with the increase in curing time, the compressive strength, flexural strength, tensile strength, and modulus of elasticity of UHPC all increase. In the case of industrial quartz sand with mineral admixture, the compressive strength, flexural strength, tensile strength, and modulus of elasticity of UHPC are generally higher than in the other cases. For standard quartz sand, the influence amplitude on the tensile strength of UHPC is initially large and then becomes smaller over time. Industrial quartz sand shows negative effects on the tensile strength of UHPC, which is unfavorable for the UHPC structure.

Table 4. Effect of mineral admixture on compressive strength and flexural strength of UHPC

Working condition	Compressive strength (MPa)			Flexural strength (MPa)		
	3day	7day	28day	3day	7day	28day
Standard quartz sand+ Blank specimen	127.1	128.9	129.6	33.2	41.5	32.8
Standard Quartz Sand+ Mineral Admixtures	120.1	137.6	138.6	33.8	38.3	37.6
Industrial quartz sand+ Blank specimen	79.5	111.8	117.8	27.1	34.2	36.1
Industrial Quartz Sand+ Mineral Admixtures	106.3	129.9	137.2	33.5	37.2	42.7

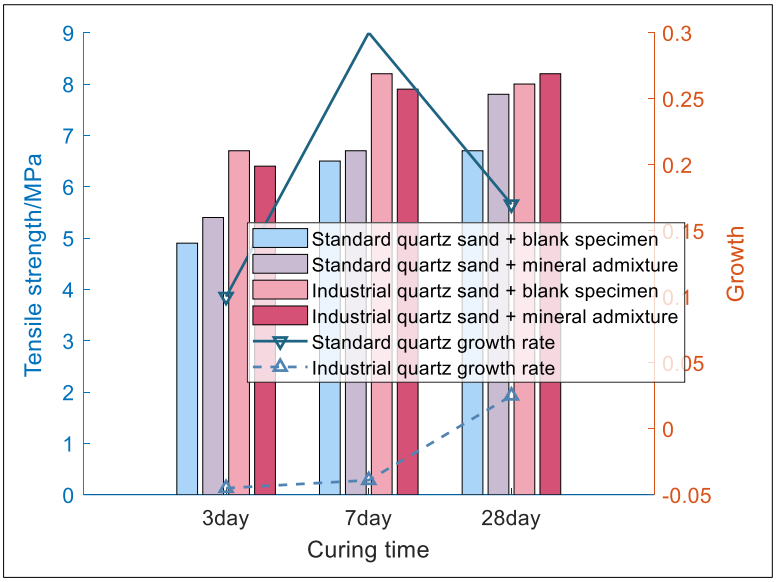

Figure 10. Effect of mineral admixture on tensile strength of UHPC

Table 5. Effect of mineral admixture on the elastic modulus of UHPC

Working condition	Modulus of elasticity (GPa)		
	3day	7day	28day
Standard quartz sand+ Blank specimen	37.6	45.2	47.9
Standard Quartz Sand+ Mineral Admixtures	47.9	52.6	53.6
Industrial quartz sand+ Blank specimen	36.2	47.5	47.2
Industrial Quartz Sand+ Mineral Admixtures	39.1	39.7	54.2

3.3. UHPC Durability Analysis

The UHPC durability analysis study focuses on UHPC durability under three environmental conditions, such as anti-chlorine ion penetration, sulfate erosion resistance, and frost resistance, as follows:

3.3.1. Analysis of Resistance to Chloride Permeation

The electrical flux of UHPC under standard and high-temperature curing conditions was analyzed by designing an anti-chlorine ion penetration experiment, and the specific results are shown in Figure 11. From Figure 11, it can be seen that the electric flux of UHPC increases with the increase of time under standard and high-temperature curing conditions; the electric flux of UHPC under standard curing conditions is higher than that under high-temperature curing conditions. From this analysis, it can be seen that the chlorine ion permeation resistance of UHPC under high-temperature curing conditions is better than that of standard curing conditions.

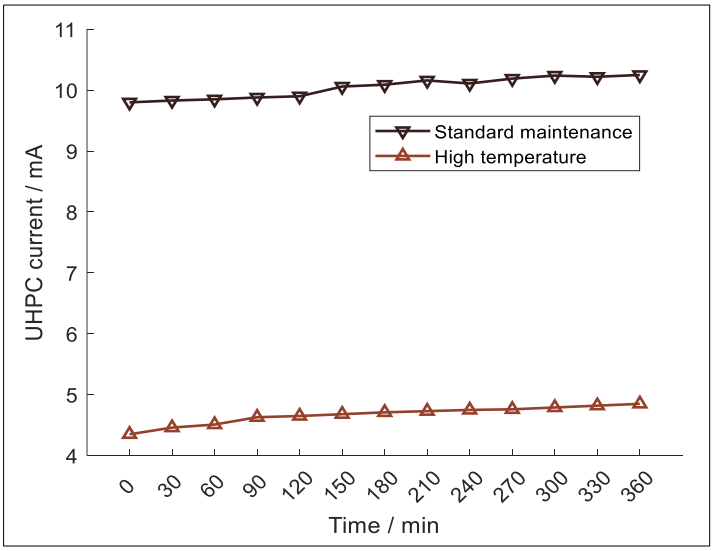

Figure 11. Results of the UHPC electric flux over time

3.3.2. Analysis of Resistance to Sulphate Erosion

To test resistance to sulfate erosion, UHPC specimens in this section were immersed in a 5% Na_2SO_4 solution and dried, using the wet–dry cycle method to analyze their resistance to sulfate attack. The specific results are shown in Figure 12. From Figure 12, it can be seen that the rate of change in the mass of UHPC specimens is basically the same under both standard curing and high-temperature curing conditions. With the increase in the number of wet–dry cycles, the mass change of the UHPC specimens first increases and then decreases. When the number of wet–dry cycles reaches 90, the mass loss of the UHPC specimens becomes evident. After 90 cycles, high-temperature curing reduces the rate of mass loss.

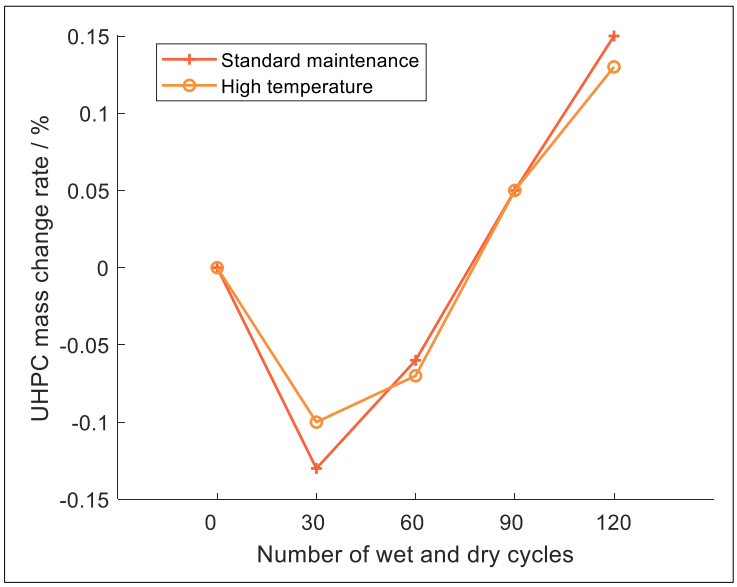

Figure 12. Changes in mass of UHPC specimens with different numbers of dry and wet cycles under different curing conditions

3.3.3. Frost Resistance Analysis

In this section, the rapid freezing method was used to test and analyze frost resistance. In this experiment, freeze–thaw cycling was started after 28 days of standard and high-temperature curing. The rate of mass change of UHPC specimens was analyzed after 100, 200, 300, 400, and 500 cycles, and the specific results are shown in Figure 13. From Figure 13, it can be seen that after both standard and high-temperature curing, the rate of mass change of UHPC specimens increases with the number of freeze–thaw cycles, and the rate under standard curing is higher than that under high-temperature curing. It can be concluded that high-temperature curing is beneficial for the UHPC structure.

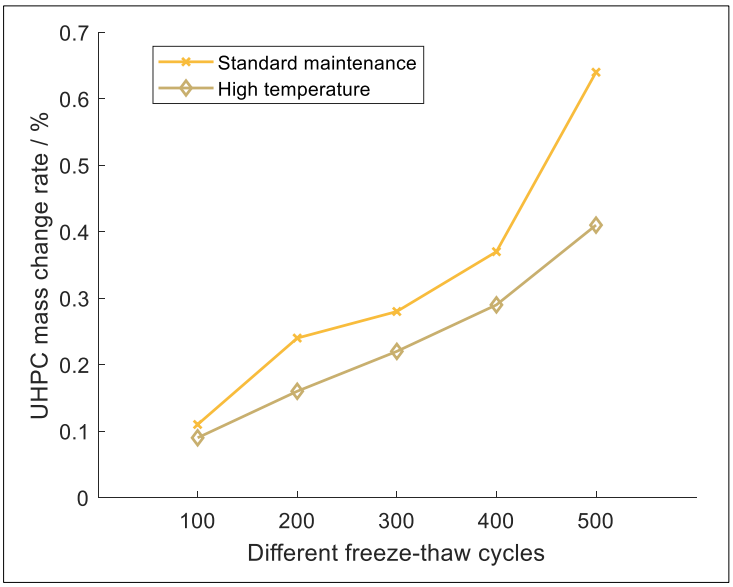

Figure 13. Changes in mass of UHPC specimens with different numbers of freeze-thaw cycles under different curing conditions

All accelerated tests were conducted in accordance with ASTM C666 (freeze–thaw) and NT BUILD 443 (chloride diffusion). Composite specimens of 0.5 m³ were exposed to a 3% NaCl + 5% Na_2SO_4 solution under temperature cycles ranging from −10 °C to +20 °C and 95% relative humidity to reproduce the coupled sea-fog and freeze–thaw conditions typical of the Bohai Sea winter environment. The in-situ monitoring section was located on a 30 m-high pier at the Port of Dalian and was exposed for 14 months, with a chloride surface deposition rate of 0.45 $kg \cdot m^{-2} \cdot a^{-1}$. After Arrhenius extrapolation, the chloride ion flux agreed with the accelerated test results within 8%.

In addition to the aforementioned properties, the cost of UHPC is also an important factor to consider. According to the data, the material cost of UHPC is approximately 650 USD per cubic metre—about 7.2 times that of conventional C50 concrete (90 USD/m³). However, because the cross-section can be reduced by 45% and steel reinforcement by 30%, the overall construction cost for a 30 m span girder decreases to only 1.8 times that of the conventional solution. Increasing the local replacement rate of cement with fly ash and slag to 40% further lowers the cost by 12%, giving UHPC initial potential for adoption in middle-income countries. A cradle-to-gate analysis based on ISO 14064 indicates that UHPC emits 580 kg of CO_2per cubic metre (including 25% silica fume), which is 66% more than C50 concrete (350 kg). However, when its maintenance-free 100-year service life is considered, the annualized emissions drop to only 34% of those for C50 concrete. Replacing 30% of the cement with calcined clay further reduces the carbon footprint to 480 kg/m³.

4. Evaluation Method for structural performance of UHPC bridges

In performance evaluation of UHPC bridges, the input feature set simultaneously includes high-dimensional, nonlinear, and non-monotonic variables such as curing temperature, sand type, mineral-admixture ratio, chloride diffusion coefficient, sulfate mass-loss rate, and freeze–thaw cycle counts. Classical grid search or empirical tuning is prone to local optima in such spaces. The Dream Optimization Algorithm (DOA) introduces a “dream-forget-share” mechanism that dynamically balances memory and forgetting, enabling an adaptive switch between global exploration and local exploitation in large-scale mixed discrete-continuous search spaces. The No Free Lunch theorem states that when an algorithm’s prior matches the problem structure, its expected performance exceeds that of random search. The UHPC response surface exhibits pronounced multi-modal and correlated-coupled characteristics; DOA’s strategy of “first memorizing the best and then randomly forgetting dimensions” aligns well with this structure. Consequently, the algorithm converges to superior hyperparameter combinations within limited iterations. In our experiments, DOA-RF reduced the out-of-bag error to 0.028 after only 100 generations, significantly outperforming PSO-RF (0.041) and GWO-RF (0.037), thereby confirming DOA’s structural suitability for high-dimensional nonlinear optimization of UHPC problems.

4.1. Introduction to Performance Evaluation Algorithms

4.1.1. Random Forest

Random Forest (Random Forest) [26] is an integrated learning method that improves the accuracy and robustness of a model by constructing multiple decision trees and combining their predictions. It is widely used for classification and regression tasks. The main steps of RF are as follows:

Self-sampling: random samples are drawn from the training set (with put-back) to generate multiple subsets;

Construct a decision tree: train a decision tree for each subset, and randomly select some features when splitting.

Voting or averaging: in classification tasks, the final result is decided by voting; in regression tasks, the final prediction is obtained by averaging.

Based on the above steps, the RF flowchart is shown in Figure 14.

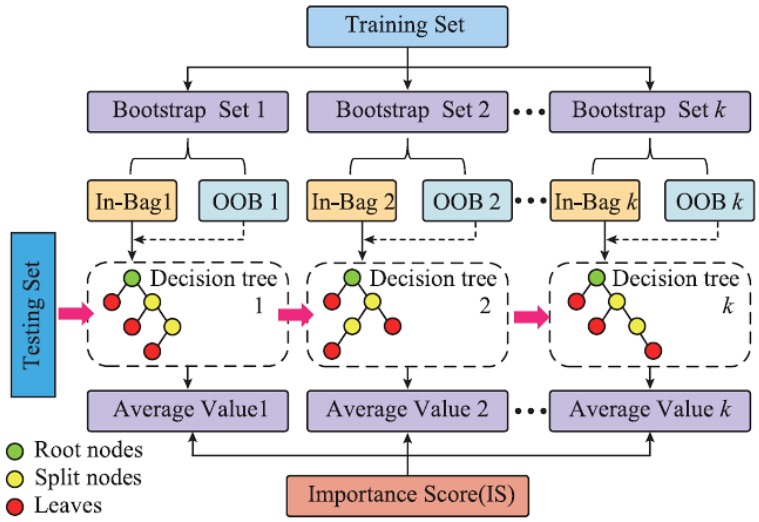

Figure 14. Random forest algorithm flow

4.1.2. Dream Optimization Algorithm

Dream Optimization Algorithm (DOA) [27] is a new meta-heuristic algorithm for solving optimization problems inspired by human dreaming behavior. The DOA-inspired principle is mainly derived from dreams, which are characterized by partial memory retention, forgetfulness, and logical self-organization, which have strong similarities with the optimization process in meta-heuristic algorithms.

Initialization: As with the other algorithms, random initialization is used:

$$X_i = X_l + \text{rand} \times (X_u - X_l) \;\; i = 1, 2 \;\cdots\; N \tag{1}$$

Where X_l and X_u denote the lower and upper bounds of the optimization variables, respectively. X_i denotes the ith DOA algorithm individual, and r denotes a random number between 0 and 1.

Exploration phase: In the exploration phase, the population is first divided into 5 groups based on differences in memory capacity, and the individuals in each group are updated as follows: each iteration is considered as a dreaming behavior, and the optimal solution and optimal value are sought by continuously executing the behavior. Before each dream, everyone in each group saw the best dream before.

Memory strategies: As the basic memory strategy suggests, for individuals in a group, they can remember the location information of the best individual in the group before dreaming, resetting their own location information to that of the best individual in the group:

$$X_i^{t+1} = X_{\text{bestq}}^t \tag{2}$$

where, X_{bestq}^t indicates the position of the best individual in the group.

Forgetting and Complementary Strategies The forgetting and complementary strategies combine global and local search functions. This strategy follows a memory strategy that allows individuals to forget and self-organize location information in the forgetting dimension. The updating equation is as follows:

$$x_{i\,j}^{t+1} = x_{best q\,j}^{t+1} + \left(x_{l\,j} + \text{rand} \times \left(x_{u\,j} - x_{l\,j}\right)\right) \times \frac{1}{2} \times \left(\cos\left(\pi \times \frac{t + T_{\max} - T_d}{T_{\max}}\right) + 1\right), \quad j = K_1 \; K_2 \; \cdots \; K_{k_q} \tag{3}$$

where, $T_{\max}$ is the maximum number of iterations, and t is the current number of iterations.

Dream sharing strategy: The dream sharing strategy in DOA enhances the escape of local optimal solutions. This strategy operates in parallel with the forgetting and complementary strategies and follows the memory strategy that allows individuals to randomly obtain location information from other individuals in the forgetting dimension. The updated equation is as follows:

$$x_{i\,j}^{t+1} = \begin{cases} x_{m\,j}^{t+1} & m \le i \\ x_{m\,j}^{t} & i < m \le N \end{cases} \qquad j = K_1, \; K_2 \; \cdots \; K_{k_g} \tag{4}$$

Development phase: Grouping is no longer performed during the development phase. Before each dream, the best dream from the previous iteration (i.e., the best individual from the previous iteration) is shown to all. Then, the position of each individual in the forgetting dimension is updated. All individuals have the same number of forgetting dimensions

① Memory strategies:

$$X_i^{t+1} = X_{\text{best}}^t \tag{5}$$

where, X_{best}^t denotes the location of the best individual.

② Forgetting and Complementary Strategies:

$$x_{i\,j}^{t+1} = x_{best\,j}^{s+1} + \left(x_{l\,j} + \text{rand} \times \left(x_{u\,j} - x_{l\,j}\right)\right) \times \frac{1}{2} \times \left(\cos\left(\pi \times \frac{t}{T_{\max}}\right) + 1\right), \quad j = K_1, \; K_2 \; \cdots \; K_{k_r} \tag{6}$$

4.1.3. DOA-RF Model Construction

To improve the evaluation performance of the RF algorithm, this paper uses the DOA algorithm to optimize and enhance RF parameters. The RF model takes RF parameters as optimization variables, UHPC structural experimental performance evaluation accuracy as the fitness value, and the DOA optimization strategy as an iterative process to construct the UHPC structural performance evaluation model. A stratified 5-fold cross-validation was employed, with each fold partitioned into training70%–validation15%–test15% sets. Iterations were terminated early if the out-of-bag (OOB) error on the validation set failed to decrease for 20 consecutive generations within 100 generations [28]. Sensitivity analyses revealed that once the number of decision trees exceeded 14 and the maximum depth exceeded 5, the reduction in mean-squared error (MSE) was less than 1%, indicating no overfitting risk.

4.2. Performance Evaluation System Construction

According to the analysis of the mechanical properties and durability of UHPC, this paper constructs evaluation indices from both aspects, including mechanical properties and durability, from the perspectives of maintenance temperature, sand type, mineral admixture, resistance to chloride penetration, resistance to sulphate erosion, and resistance to freezing, as shown in Figure 15.

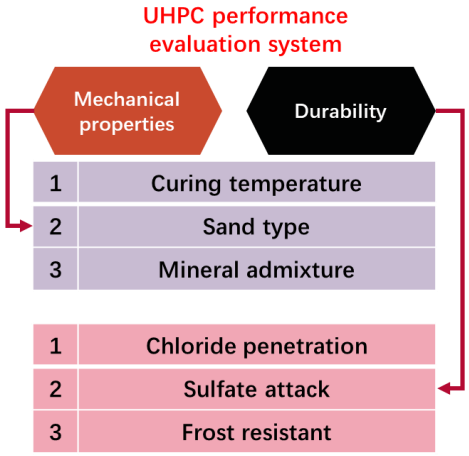

Figure 15. UHPC performance evaluation system

4.3. Methodological Steps

Combining the performance evaluation system and DOA-RF model, the flowchart of the UHPC performance evaluation method based on the DOA-RF algorithm is shown in Figure 16 with the following steps:

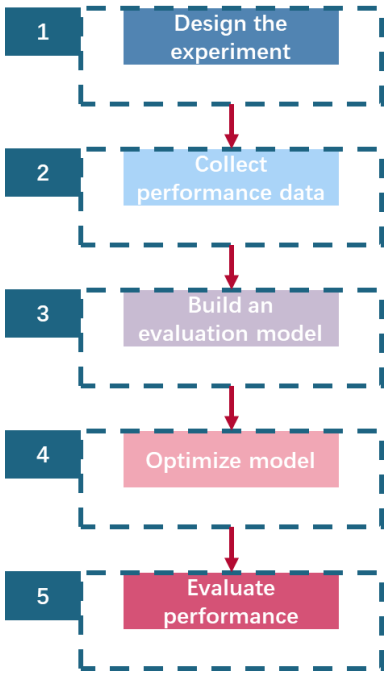

Figure 16. UHPC performance evaluation method based on the DOA-RF algorithm

Step 1: Design UHPC bridge structure mechanics and durability tests under different environments. Through the mixing process selection method, design the UHPC bridge structure mechanical test in terms of maintenance temperature, sand type, and mineral admixture, and design the UHPC bridge structure durability test in terms of chlorine ion penetration resistance, sulfate erosion resistance, and frost resistance.

Step 2: Collect statistical UHPC bridge structure performance data. Obtain UHPC bridge structure mechanical and durability performance data by conducting mechanical and durability tests to construct a sample set of UHPC bridge structures.

Step 3: Construct the performance evaluation model. Using the RF algorithm, learn to train the UHPC bridge structure sample set and construct the UHPC bridge structure performance evaluation model based on the RF algorithm.

Step 4: Optimize the model. The parameters of the RF algorithm are optimized using the DOA algorithm to improve the UHPC bridge structural performance evaluation model.

Step 5: Evaluate the performance evaluation model. The model results are analyzed and compared from multiple perspectives using a test set.

5. Performance Evaluation Analysis

5.1. Analyzing the Design of the Environment

The performance testing environment of this paper is set as follows: operating system: 64-bit Windows 10; processor: Intel Core i7, simulation software: Matlab2020a, and comparison algorithm parameter settings:

- RF algorithm: n_estimators=10, max_features=4, max_depth default value, min_samplesleaf=3;
- PSO-RF algorithm: the parameters of the RF algorithm were optimized using the PSO algorithm with a population size of 50, an iteration number of 100, inertia weight w = 0.7, and cognitive and social factors of 0.25 and 0.25, respectively;
- GWO-RF algorithm: the parameters of the RF algorithm were optimized using the GWO algorithm with a population size of 50, an iteration number of 100, and a control parameter of 2, which decreases linearly with the number of iterations;
- DE-RF algorithm: the parameters of the RF algorithm were optimized using the DE algorithm with a population size of 50, an iteration count of 100, a crossover rate of 0.7, and a variance rate of 0.6;
- DOA-RF algorithm: the parameters of the RF algorithm were optimized using the DOA algorithm with 50 populations and 100 iterations.

5.2. Analysis of Results

5.2.1. UHPC Micro Effects in Different Environments

In order to further analyze the mechanical and durability properties of UHPC in different environments, this paper analyzes them from a microscopic perspective, with the specific results shown in Figures 17 to 20.

Figure 17 gives the electron microscope images of UHPC test pieces at 28d under different curing environments. As can be seen from Figure 17, after the UHPC test pieces are under the standard curing environment, there are many disordered distributions of particles, and there are also some hexagonal lamellar CH crystals that are not fully involved in the secondary hydration, and these phenomena are mainly because the cement can't be fully hydrated; after the high-temperature curing environment, the hydration of the UHPC test pieces is accelerated, and a large amount of C-S-H gels are generated, and the Aft that is different from the water is generated. The void area of the UHPC test specimens in the high-temperature curing environment is decreasing compared with that of the standard curing environment.

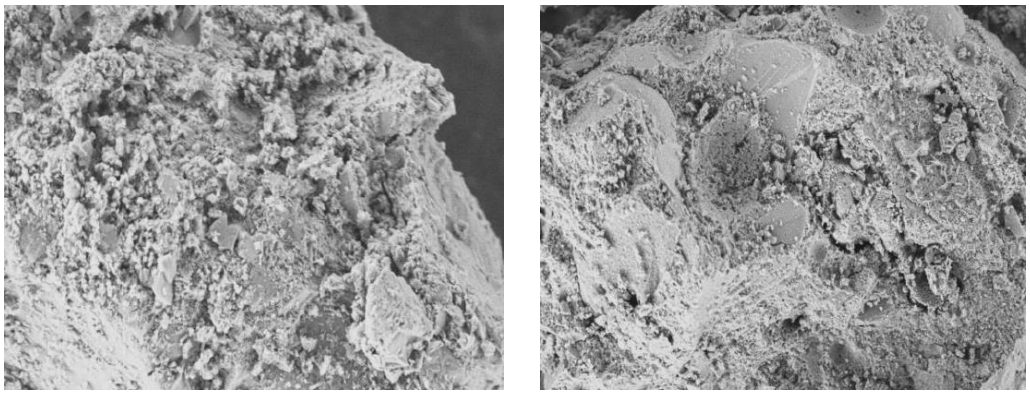

(a) Under standard conservation conditions (b) High-temperature conservation conditions

Figure 17. Electron microscope images of UHPC test pieces at 28d under different conservation environments

Figure 18 gives an electron microscope image of the UHPC test piece after the impermeability test. As can be seen from Figure 18, no obvious cracks appeared in the UHPC test pieces after the impermeability test, which proved that the test pieces had good impermeability performance, consistent with the results of the test on the resistance to chlorine ion permeability.

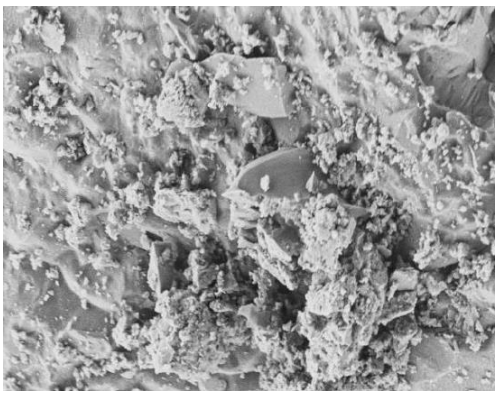

Figure 18. Electron microscope image of UHPC test piece after impermeability test

An electron microscope image of the UHPC test piece after 120 wet and dry cycles is given in Figure 19. The UHPC test piece showed no obvious cracks, and the number of internal CH crystals was reduced.

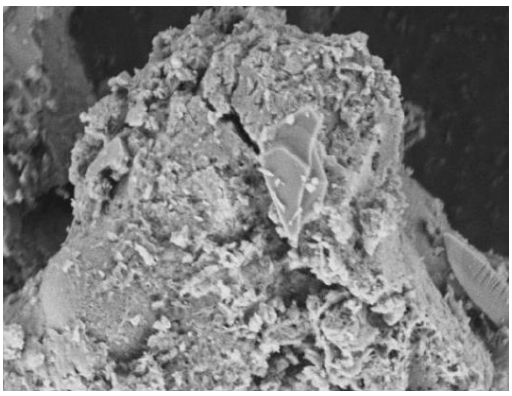

Figure 19. Electron microscope image of UHPC test piece after 120 wet and dry cycles

An electron microscope image of the UHPC test piece after 500 freeze-thaw cycles is given in Figure 20. The UHPC test piece showed more obvious transverse cracks, which damaged the structure of the UHPC matrix and caused its strength to decrease, thus causing the test piece to fail.

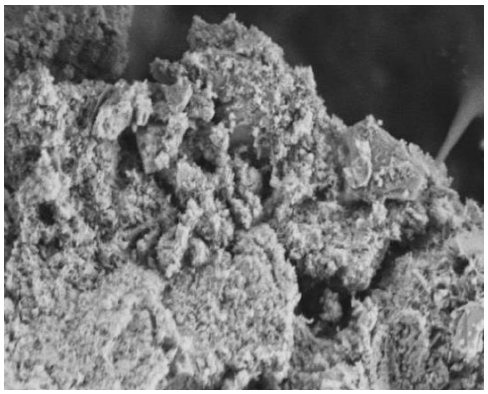

Figure 20. Electron microscope image of UHPC test piece after 500 freeze-thaw cycles

5.2.2. Evaluation Performance Analysis

In order to verify the comparative analysis of the DOA-RF algorithm in the UHPC performance evaluation effect, this paper uses the RF algorithm, PSO-RF algorithm, GWO-RF algorithm, DE-RF algorithm, and DOA-RF algorithm to compare the specific results as shown in Figure 21 and Table 6.

Figure 21 demonstrates the comparative results of different performance evaluation algorithms for the structural performance assessment of UHPC bridges, mainly including DOA-RF (Dreaming Optimization - Random Forest), DE-RF (Differential Evolution - Random Forest), GWO-RF (Grey Wolf Optimization - Random Forest), PSO-RF (Particle Swarm Optimization - Random Forest), and traditional RF (Random Forest) algorithms. In terms of the MSE (Mean Squared Error) and R^2 (Coefficient of Determination) metrics, the DOA-RF algorithm has the lowest MSE, indicating

that it has the smallest prediction error, while R^2 is the highest (up to 0.75), which suggests that its prediction results have the best fit to the actual data. In contrast, the unoptimized RF algorithm has the highest MSE and the lowest R^2, indicating a poorer assessment, while DE-RF, GWO-RF, and PSO-RF show some improvement but still fall short of the optimized level of DOA-RF. The superiority of DOA-RF is mainly attributed to the efficient parameter optimization capability of the Dream Optimization Algorithm (DOA), which allows Random Forest to be used in predicting the UHPC material performance with more precise parameter tuning, improving the generalization ability and evaluation accuracy of the model. In addition, DOA-RF shows great adaptability in the complex performance prediction of UHPC materials, which can effectively reduce the prediction error and improve the reliability of performance assessment of UHPC structures under different environmental conditions. Therefore, the DOA-RF algorithm performs best in the performance evaluation of UHPC bridge structures, providing accurate data support for optimizing UHPC material equations, construction processes, and structural design, and laying the foundation for intelligent engineering material evaluation in the future.

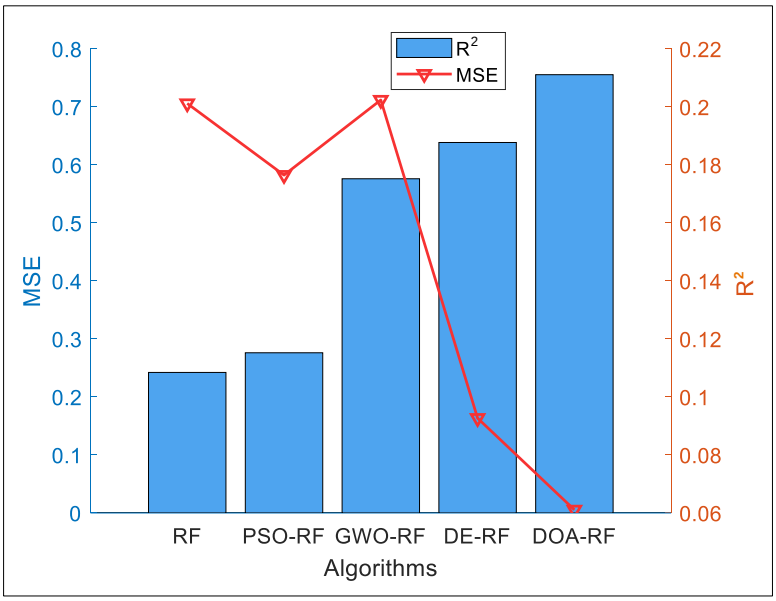

Figure 21. Evaluation results of different UHPC performance evaluation methods

Table 6 shows the hyper-parameter optimization results of different performance evaluation algorithms (RF, PSO-RF, GWO-RF, DE-RF, DOA-RF) for the structural performance evaluation of UHPC bridges, which mainly include three key parameters: the number of decision trees, the maximum number of features, and the maximum depth of the tree. From the data in Table 6, it can be seen that the optimized DOA-RF algorithm has several decision trees of 14, a maximum number of features of 4, and a maximum depth of 5, which are the best parameter settings among all the algorithms, resulting in the best performance in terms of the MSE and R^2 metrics in Figure 21. In contrast, the traditional RF algorithm has a decision tree count of only 10 and a maximum tree depth of only 3, resulting in a larger prediction error and lower goodness-of-fit. The optimized PSO-RF, GWO-RF, and DE-RF algorithms improved in parameter tuning, e.g., the number of decision trees was increased to 20 for DE-RF, and the tree depth reached 7 for GWO-RF, but they still failed to reach the optimal configuration of DOA-RF. The ability of DOA-RF to achieve higher prediction accuracies with fewer decision trees and appropriate tree depths is mainly due to the Dream State Optimization Algorithm (DOA)'s precise tuning of the hyperparameters, which provides the model with better generalization capabilities in complex UHPC performance evaluation tasks [29]. In addition, the optimized parameter settings of DOA-RF not only reduce the computational cost of the model but also enhance the assessment efficiency, making it more suitable for intelligent prediction, structural optimization, and construction quality control of UHPC materials. Therefore, the results in Table 6 further verify the superiority of the DOA-RF algorithm in the structural performance assessment of UHPC bridges and provide a more reliable optimization strategy and technical support for practical engineering applications.

Table 6. Parameter results of different evaluation algorithms

No.	Hyper parameterization	Realm	RF	PSO-RF	GWO-RF	DE-RF	DOA-RF
1	Number of decision trees	1~100	10	16	31	20	14
2	Maximum number of features	3~50	4	10	4	3	4
3	Maximum depth of the tree	3~10	3	6	7	8	5

6. Conclusions

In this study, the application of ultra-high-performance concrete (UHPC) in bridge structures is comprehensively analyzed, focusing on the mechanical properties and durability of UHPC under different environmental conditions. Through detailed test preparation and accurate simulation, combined with on-site monitoring data, this paper adopts advanced Random Forest and Dreamland optimization algorithms to systematically evaluate the performance of UHPC. The following conclusions were obtained through the experimental analyses:

- Comparing the two maintenance temperatures, high-temperature maintenance can improve the mechanical properties of UHPC, reduce the value of resistance to chlorine penetration current, increase the resistance to sulfate erosion, and reduce the frost resistance after a freeze-thaw cycle;
- Comparing the evaluation results of different evaluation algorithms, the DOA-RF algorithm MSE value has decreased, and the R^2 coefficient has increased;
- The DOA-RF algorithm solves the problem of evaluating the mechanical properties and durability of UHPC.

The research results in this paper provide theoretical guidance for the engineering application of UHPC materials, and it is recommended that future research continue to deepen the research on the performance of UHPC under the action of extreme climatic and composite environments in order to promote its sustainable application in bridge engineering.

However, there are some limitations to the study. Firstly, although this study covers a wide range of environmental conditions, the effects of extreme conditions such as ultra-low temperatures have not been thoroughly investigated. Second, the high cost and complex construction techniques of UHPC are still important factors limiting its widespread use in practical applications. Therefore, these issues need to be addressed in future research.

Going forward, research will continue to explore the application of UHPC in a wider range of environmental conditions, particularly in light of the potential impact of global climate change on the performance of bridge materials. At the same time, research will endeavor to reduce the cost of UHPC production and simplify the construction process to make it more suitable for large-scale infrastructure projects. In addition, the development of new UHPC equations to improve its environmental resilience and sustainability will also be a focus of future research. In the future, UHPC could be integrated with distributed optical fiber sensing (DOFS) and carbon nanotube (CNT) self-sensing networks to enable real-time monitoring of chloride ion concentration and crack width. Preliminary tests show that UHPC containing 0.5 wt % CNT exhibits a linear relationship ($R^2 = 0.92$) between the resistivity change rate and crack width, offering a new pathway for enhancing bridge resilience and enabling predictive maintenance. Through these efforts, it is expected that UHPC will play an even more critical role in future bridge projects.

7. Declarations

7.1. Data Availability Statement

The data presented in this study are available in the article.

7.2. Funding

This work was supported by the Research on the Application of Intelligent Management Evaluation Technology in Engineering Quality, Safety, and Environmental Protection (No.29024266).

7.3. Institutional Review Board Statement

Not applicable.

7.4. Informed Consent Statement

Not applicable.

7.5. Declaration of Competing Interest

The author declares that they have no known competing financial interests or personal relationships that could have appeared to influence the work reported in this paper.

8. References

[1] Su, J., Li, J., Chu, S., Wu, D., Ma, J., & Li, Z. X. (2025). Assessment of seismic performance for ultra-high performance concrete (UHPC) retrofitted RC bridge piers with height-varying corrosion: A lifetime perspective. Engineering Structures, 339, 120693. doi:10.1016/j.engstruct.2025.120693.

[2] Li, Y., Li, Z., Luo, Z., & Yu, N. (2024). Research and application of rapid reconstruction technology to existing bridge guardrails based on UHPC connection. Advances in Bridge Engineering, 5(1), 24. doi:10.1186/s43251-024-00135-3.

[3] Jia, J., Ren, Z., Bai, Y., Li, J., Li, B., Sun, Y., Zhang, Z., & Zhang, J. (2023). Tensile behavior of UHPC wet joints for precast bridge deck panels. Engineering Structures, 282, 115826. doi:10.1016/j.engstruct.2023.115826.

[4] Yang, W. (2024). Introduction to the 180-Meter UHPC Mixed Tower Structure Wind Power Project in Lianshui, Jiangsu. Prestress Technology, 2(02), 81–85. doi:10.59238/j.pt.2024.02.007.

[5] Zhao, Q., Yang Y. F, Jing, B. R., & Ruan, F. R. (2024.). Design method of fibre continuous wet joints for prefabricated UHPC bridge deck slabs. Engineering Mechanics, 42, 1-16. doi:10.6052/j.issn.1000-4750.2024.03.0203.

[6] Gao, L. Q., Yu, L. H., & Wang, K. N. (2023). Comparison of fatigue assessment methods for steel-UHPC bridge decks between Chinese and foreign specifications. Bridge Construction, 53(05), 74-82. doi:10.20051/j.issn.1003-4722.2023.05.010.

[7] Chen, H., Zhang, G., Ding, Q., Yang, J., Zhu, J., & Qi, D. (2025). Effect of expansive agent on lightweight micro-expansive ultra-high performance concrete: Properties, microstructure, and interfacial bonding in concrete-filled steel tube. Construction and Building Materials, 462(2). doi:10.1016/j.conbuildmat.2025.139996.

[8] Chen, H., Zhang, G., Ding, Q., Zhu, J., Yang, J., Fu, J., & Wang, Y. (2025). Effect of lightweight aggregate pre-wetting degree on the chloride ion permeability of ultra-high performance concrete. Journal of Building Engineering, 100. doi:10.1016/j.jobe.2025.111777.

[9] Xu, G., Xu, W., Dong, X., Fan, S., & Wang, X. (2023). Characteristics of Corrosion Products of Friction-Type High-Strength Bolted Joints of Steel Bridge: A Case Study. Coatings, 13(6). doi:10.3390/coatings13061023.

[10] Chen, Y., Tong, J., Li, Q., Xu, S., & Shen, L. (2024). Application of High-Performance Cementitious Composites in Steel-Concrete Composite Bridge Deck Systems: A Review. Journal of Intelligent Construction, 2(2), 1–23. doi:10.26599/jic.2024.9180012.

[11] Wakjira, T. G., & Alam, M. S. (2024). Performance-based seismic design of Ultra-High-Performance Concrete (UHPC) bridge columns with design example – Powered by explainable machine learning model. Engineering Structures, 314, 118346. doi:10.1016/j.engstruct.2024.118346.

[12] Hong, L., Li, Z., & Peng, Y. (2024). Application of lightweight steel-UHPC composite beam in bridge emergency repair. Advances in Bridge Engineering, 5(1). doi:10.1186/s43251-024-00128-2.

[13] Deng, S., Huang, Z., Xiao, G., & Shen, L. (2023). Modeling the transverse connection of fully precast steel-UHPC lightweight composite bridge. Advances in Concrete Construction, 15(6), 391–404. doi:10.12989/acc.2023.15.6.391.

[14] Li, S., Li, H., Cheng, Z., Wang, J., Alam, M. S., & Yao, Y. (2023). Cyclic Loading Test and Numerical Modeling on Prefabricated UHPC Tube–Confined Rectangular Bridge Piers with Different Base Connections. Journal of Structural Engineering, 149(10), 04023135. doi:10.1061/jsendh.steng-11875.

[15] Gil, A., & Kodur, V. (2023). Evaluating Shear Response of UHPC Bridge Girders Exposed to Fire. Fire Technology, 60(4), 2349–2372. doi:10.1007/s10694-023-01506-4.

[16] Li, X., Li, R., & Hu, Z. (2024). Bearing capacity of UHPC-NC connection structure in negative moment zone of PC beam bridges. Structural Concrete, 25(2), 796–809. doi:10.1002/suco.202300278.

[17] Farhoud, H., Mackin, A., & Mantawy, I. M. (2025). Novel external dissipative device for rocking bridge columns: Resilient rotational friction elements. Structures, 78(1), 109317. doi:10.1016/j.istruc.2025.109317.

[18] Wang, X., Qin, Z., Bai, X., Hao, Z., Yan, N., & Han, J. (2025). Research Progress of Machine Learning in Deep Foundation Pit Deformation Prediction. Buildings, 15(6), 852. doi:10.3390/buildings15060852.

[19] Tan, C., Luo, Z., Zhao, H., An, J., Liang, L., Guo, W., & Shao, X. (2023). Flexural Behavior on a Steel–UHPC Composite Deck System of Long-Span Bridges. Journal of Bridge Engineering, 28(9), 04023062. doi:10.1061/jbenf2.beeng-6323.

[20] Zhang, Z., Guan, Z., Ge, W., Liu, Y., Li, S., & Cao, D. (2024). Flexural Performance of SSK Reinforced Steel–UHPC Composite Beams: Experimental and Numerical Study. Journal of Bridge Engineering, 29(2), 05023012. doi:10.1061/jbenf2.beeng-6493.

[21] Xu, T., Yang, J., Wang, C., Guo, T., Deng, K., & Xie, T. (2024). Comparative sustainability and seismic performance analysis of reinforced conventional concrete and UHPC bridge piers. Journal of Cleaner Production, 467, 142959. doi:10.1016/j.jclepro.2024.142959.

[22] Huang, X., Yang, Y., Fu, X., Liao, M., & Huang, S. (2025). Structural behavior of shear-dominant externally prestressed UHPC T-shaped beams. Structures, 71, 107950. doi:10.1016/j.istruc.2024.107950.

[23] Zhu, J., Liu, Z., Liu, X., Li, L., & Li, Y. (2024). Bending performance of wet joints in negative moment zone of prefabricated small-box girder bridges: Experimental and numerical study. Structures, 62, 106103. doi:10.1016/j.istruc.2024.106103.

[24] Zhu, J., Tong, X., Li, Y., & Li, L. (2024). Research on flexural behavior and design method of formwork free UHPC wet joint in prefabricated small box girder bridges. Structures, 69, 69. doi:10.1016/j.istruc.2024.107333.

[25] Fu, T., Wang, K., Zhu, Z., Ren, X., Li, Y., Xu, L., Meng, L., & Sun, Z. (2023). Seismic performance of prefabricated square hollow section piers strengthened by jacketing using UHPC and high-strength steel. Structures, 47, 449–465. doi:10.1016/j.istruc.2022.11.077.

[26] Ai, Z., Liu, H., Zhang, J., Zhang, C., Wang, C., Jiang, Z., & Xiao, R. (2023). Study on The Mechanical and Economic Performance of Super Long-Span Cable-Stayed Bridges with UHPC-Girder. KSCE Journal of Civil Engineering, 27(11), 4744–4761. doi:10.1007/s12205-023-0835-0.

[27] Liu, K., Zhong, H., & Lin, W. (2024). Tree Species Classification in UAV Hyperspectral Images Based on Different Machine Learning Algorithms. Forest Engineering, 40(4), 98–108. doi:10.7525/j.issn.1006-8023.2024.04.011.

[28] Luyao, W., Xingke, C., & Haijun, Z. (2024). Durability assessment of continuous concrete girder bridges based on Random Forest and hierarchical analysis. Journal of Shenyang University (Natural Science Edition, 36(3), 255–261.

[29] Lang, Y., & Gao, Y. (2025). Dream Optimization Algorithm (DOA): A novel metaheuristic optimization algorithm inspired by human dreams and its applications to real-world engineering problems. Computer Methods in Applied Mechanics and Engineering, 436, 117718. doi:10.1016/j.cma.2024.117718.